

FULL-SCALE TESTING AND ANALYSIS OF FUSELAGE STRUCTURE

M. Miller, M. L. Gruber, K. E. Wilkins, R. E. Worden
The Boeing Company, Seattle, Washington 98124

532-39
23/26
p. 16

SUMMARY

This paper presents recent results from a program in the Boeing Commercial Airplane Group to study the behavior of cracks in fuselage structures. The goal of this program is to improve methods for analyzing crack growth and residual strength in pressurized fuselages, thus improving new airplane designs and optimizing the required structural inspections for current models. The program consists of full-scale experimental testing of pressurized fuselage panels in both wide-body and narrow-body fixtures and finite element analyses to predict the results. The finite element analyses are geometrically nonlinear with material and fastener nonlinearity included on a case-by-case basis. The analysis results are compared with the strain gage, crack growth, and residual strength data from the experimental program. Most of the studies reported in this paper concern the behavior of single or multiple cracks in the lap joints of narrow-body airplanes (such as 727 and 737 commercial jets). The phenomenon where the crack trajectory is curved creating a "flap" and resulting in a controlled decompression is discussed.

INTRODUCTION

The Boeing Commercial Airplane Group has a continuing program to investigate the durability and damage tolerance of airplane structures. In the mid-1980s, the opportunity arose to build two test fixtures to study the behavior of typical fuselage structure. To complement this test program, a parallel activity to conduct finite element analyses of typical fuselage configurations was initiated. The objective is to improve our damage tolerance methods for the design and evaluation of fuselage pressure structure. This should result in safer designs and a reduced inspection burden on the operators. In recent times, the scope of the research has been extended to include assessments of the effects of multiple site damage on the residual strength of fuselage lap joints.

PRESSURE TEST FACILITY

The test facility, illustrated in Figure 1, consists of two cylindrical fixtures.

The first fixture has a radius of 74 inches (1.88 m) to match Boeing's typical narrow-body airplanes, and the second has a radius of 127 inches (3.23 m) to match the wide-body airplanes. Both fixtures are 20 feet (6.1 m) in length as shown in Figure 2. The overall geometry of the fixtures is consistent with typical fuselage design: 7075-T6 frames at a 20 inch (508 mm) pitch and 2024-T3 clad stringers at a 9.25 inch (235 mm) pitch. The frames are attached to the stringers by means of stringer clips, but are otherwise not connected directly to the skin. The skin, frame and stringer gages are thicker than typical minimum gage fuselage structure but have been selected to maintain realistic fixture stiffness. All fastener holes in the skin are cold-worked and protruding head fasteners are used to provide maximum fixture longevity. External 2.8 inch (71 mm) wide circumferential tear straps of 2024-T3 clad sheet are riveted to the skin at a 20 inch (508 mm) spacing. The end bulkheads are steel, one of which is fixed and the other on rollers to permit axial expansion during pressurization.

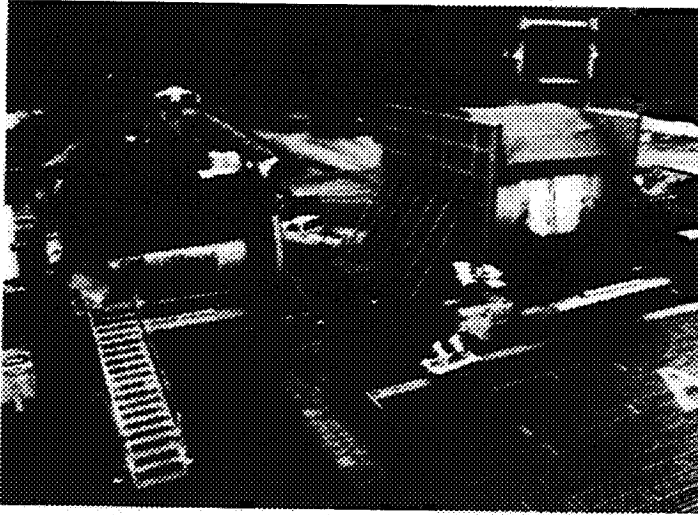


Figure 1. Pressure test site.

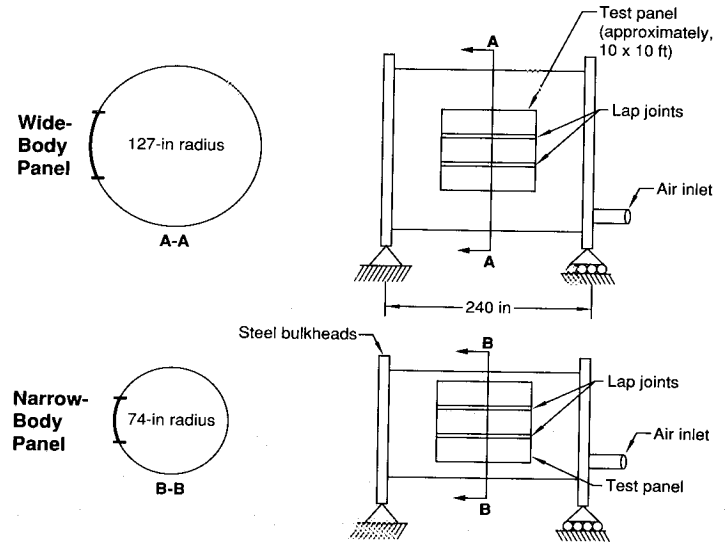


Figure 2. Schematic of pressure test fixtures.

The narrow-body fixture has a single rectangular cutout 10 feet x 10 feet (3.05 m x 3.05 m), designed to accept the test panels. Similarly, the wide-body fixture has two diametrically opposed cutouts also 10 feet x 10 feet (3.05 m x 3.05 m). The test panels are attached to the fixture at the skin, frames, and stringers by a fusing arrangement that allows the panel to fail at loads below the elastic limit of the fixture components. The stringer and frame splices are designed to allow attachment fasteners to shear during a dynamic panel failure. The test panel skin is allowed to tear circumferentially along the perimeter fasteners with the help of a sharp notch introduced into the panel prior to its installation in the fixture. With these features, it is possible to conduct residual strength tests which result in test panel failure without extensive damage to the test fixture.

Compressed air is used as the pressurizing medium. Five electric compressors are capable of producing a differential pressure of 90 psi (0.62 MPa) resulting in delivery of a nominal 1600 cubic feet (45.3 cubic meters) of air per minute. The flow of air is regulated into the fixtures by means of a digitally controlled valve. Cyclic rates are 1 minute per cycle in the narrow-body fixture and two minutes per cycle in the wide-body fixture. Polystyrene blocks are placed within the fixtures to reduce the required air volume.

To reduce air leakage during testing, 0.1 inch (2.5 mm) thick rubber air bladders are placed against the inner skin of the test panel in the vicinity of the crack. Some testing has been conducted with insulation blankets used on a commercial airplane. These have inadequate strength and durability however for long-term testing. Thin aluminum sheet, loosely attached to the interior of the skin panel, was found to affect crack growth behavior and is no longer used.

The data acquisition system consists of up to 300 channels for recording test information, principally from strain gages. Typically, rosettes are used on the skins and axial gages on the stringers, tear straps, and frame chords. Most tests are remotely monitored using video cameras. The test differential pressures are superimposed on the video image in real time. The resulting film is available for subsequent review and analysis.

TEST RESULTS

The discussion of test results is divided into two sections dealing with narrow-body and wide-body panels respectively. Experience has indicated that the behavior of each can be significantly different; there is a tendency toward controlled decompression in narrow-body panels. This results when a longitudinal crack in the skin turns to grow in the circumferential direction. A segment of the skin peels back creating an opening that prevents further pressurization. This phenomenon, often described as “flapping,” is rarely encountered in wide-body panels. It is believed to be primarily a function of skin gage, but is also influenced by initial crack location, tear strap dimensions, the presence of shear-ties and other detail design features.

Narrow-Body Tests

Four tests were conducted on narrow-body panel 74-A shown in Figure 3. In general, the test procedure consisted of inserting a 5 inch (127 mm) sawcut at the selected test location and pressure cycling until either test termination or the crack reached a length at which a residual strength test was performed. Each crack was repaired before inserting the next sawcut. The test panel is divided into two halves by a single longitudinal lap joint. All frames are “floating,” connected to the stringers only by means of stringer clips. In the upper half of the panel the skin is 0.040 inch (1.02 mm) thick, and in the lower half of the panel the skin is 0.056 inch (1.32 mm) thick. All longitudinal cracks are parallel to the longitudinal grain direction of the 2024-T3 clad skin. Internal bonded tear straps are installed at each frame location. The tear strap dimensions are defined in terms of a strap stiffening ratio:

$$R_s = A_{\text{strap}} / (B \cdot t_{\text{skin}})$$

where A_{strap} is the tear strap cross-sectional area, B is the frame spacing, and t_{skin} is the skin gage. The frame cross-sectional area is not included in the evaluation of the strap stiffening ratio.

Test 1 on this panel consisted of a longitudinal 5 inch (127 mm) sawcut adjacent to stringer 4L in the 0.056 inch (1.32 mm) skin. The strap stiffness ratio R_s was 0.14. The panel was subjected to a cyclic differential pressure of 8.6 psi (.059 MPa) with a stress ratio of zero. As is typical with sawcuts at such a location, the direction of fatigue crack growth gradually diverged from longitudinal. In this case, failure consisted of a controlled decompression as shown in Figure 4. Figure 5 shows that 5400 pressure cycles were required to grow the crack to its final length.

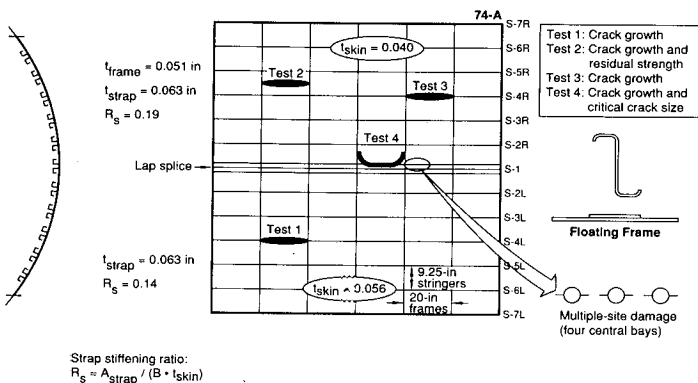


Figure 3. Initial damage locations on narrow-body panel 74-A.

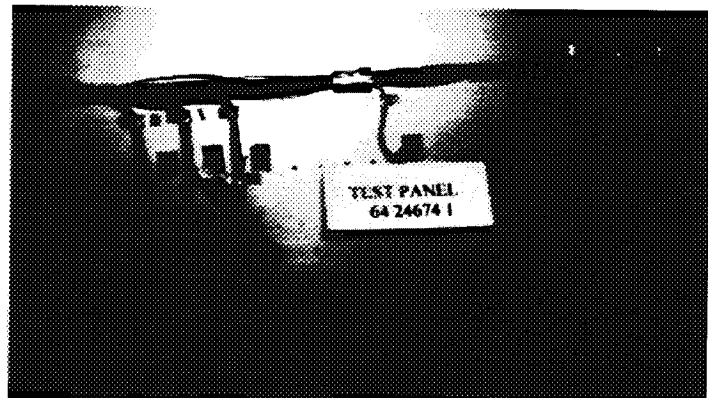


Figure 4. Final failure of Test 1 on panel 74-A.

Test 2 consisted of a longitudinal five inch (127 mm) sawcut midway between stringers 4R and 5R in the 0.04 inch (1.02 mm) skin. The strap stiffness ratio R_s was 0.19. In this case, the crack grew straight until it reached the bonded tear straps at a length of 17.4 inches (442 mm). A single pressure cycle to 10.3 psi (.071 MPa), representing the regulatory residual strength load requirement was applied without inducing significant crack extension. The test was discontinued at that time and the panel repaired.

Test 3 consisted of a longitudinal five inch (127 mm) sawcut adjacent to stringer 4R in the 0.04 inch (1.02 mm) gage skin. The direction of crack growth was similar to test 1 and resulted in a controlled decompression after 950 cycles. Comparison of the data in Figure 5 shows that the midbay crack of test 2 has a shorter crack growth life than the crack in test 3. This is consistent with data presented in Reference 1. The crack length at instability for Test 3 of 14.8 inches (380 mm) can be compared with a crack length at instability of 18 inches (460 mm) in Test 1, attributable in part to the stresses associated with the different skin gages.

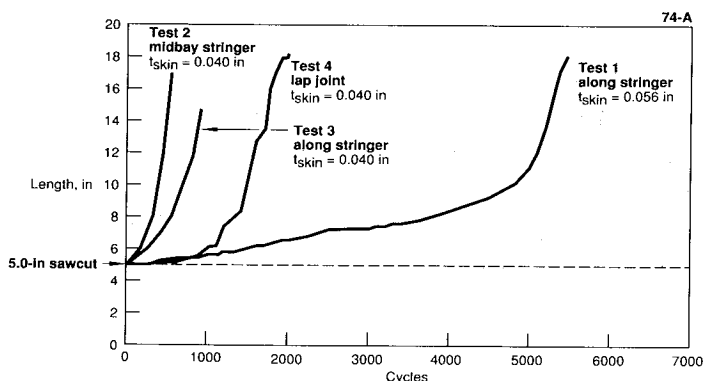


Figure 5. Crack growth test results for panel 74-A.

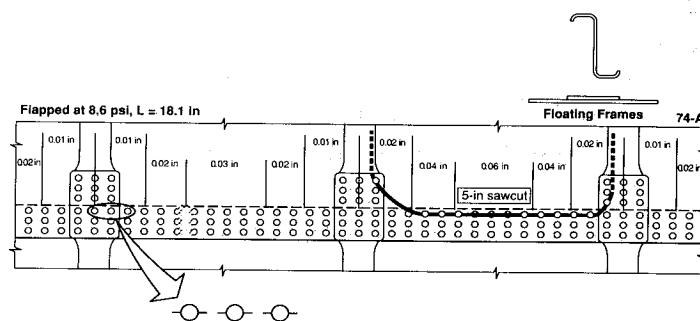


Figure 6. Multiple site damage test on panel 74-A lap joint.

Test 4, the final test in panel 74-A, consisted of a five inch (127 mm) sawcut in the upper row of fasteners in the lap joint of the 0.04 inch (1.02 mm) skin. Each fastener hole ahead of the initial sawcut had two small diametrically opposed longitudinal sawcuts introduced during original panel assembly as shown in Figure 6. The dimensions of these sawcuts varied as a function of location along the lap joint and were smaller at the tear strap locations as indicated by fleet experience. Although these small sawcuts had experienced approximately 7000 prior pressure cycles, it is unlikely that there would have been any appreciable growth prior to inserting the 5 inch sawcut in the lap joint. Initially the crack growth from the 5 inch sawcut remained in the rivet line during pressure cycling, although reference to Figure 7 shows the tendency of the crack to deviate from the longitudinal direction only to be pulled back to the rivet line at the next fastener hole. The crack finally began to grow significantly away from the rivet line as it approached the adjacent tear straps. Final failure was a controlled decompression as shown in Figure 8. Comparison of the crack growth rates in Figure 5 shows that the crack in the lap joint grew more slowly than the midbay crack of Test 2 and the crack adjacent to Stringer 4R in Test 3.

A single test was conducted on Panel 74-B. This panel differed from panel 74-A by the use of shear-ties to attach the frame directly to the skin and bonded tear strap as shown in Figure 9. In this test, the tear strap stiffening ratio R_s was 0.12. The initial condition consisted of a five inch (127 mm) sawcut along the upper fastener row of the lap joint. Again, each fastener hole ahead of the initial sawcut had two small diametrically opposed longitudinal sawcuts introduced during the original panel assembly. The secondary sawcut lengths were varied in a manner similar to those in panel 74-A. However, the panel had not been subjected to prior fatigue cycling before introduction of the 5 inch sawcut. Review of the lap joint following final failure

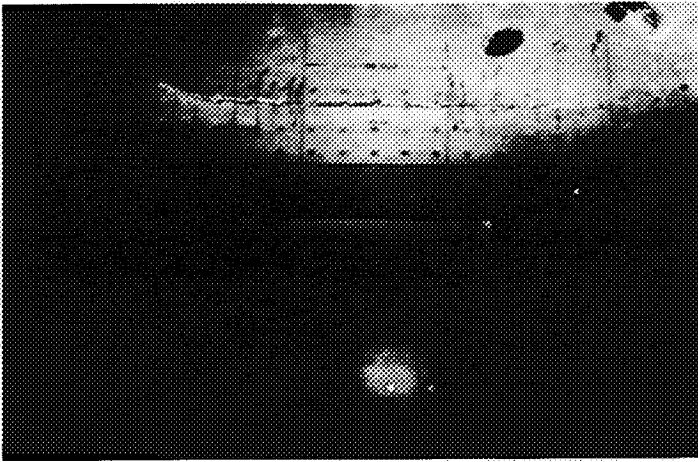


Figure 7. Crack progression during multiple site damage test on panel 74-A lap joint.

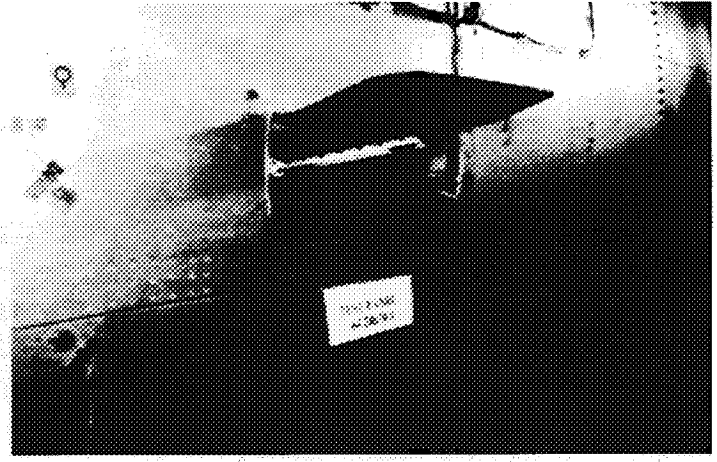


Figure 8. Final failure of multiple site damage test on panel 74-A lap joint.

revealed that several sawcuts in the same frame bay as the lead crack had grown about 0.25 inch (6 mm) during fatigue cycling. During this time, the crack showed little tendency to deviate far from the rivet line. It did however deviate from the rivet line and head toward the middle of the stringer bay as it crossed the adjacent tear straps. A fatigue crack of length 1 inch (25 mm) was detected in one of these tear straps when the skin crack was around 20 inches (510 mm) in length. This tear strap failed in fatigue when the skin crack was around 23 inches (580 mm) in length. The second tear strap failed when the skin crack was 24.5 inches (620 mm) in length. A total of 85 pressure cycles were required to fail both tear straps following the initial tear strap crack detection. The lead crack continued to grow until it reached a length of 40.2 inches (1.02 m) as shown in Figure 10. At this time, unstable crack extension resulted leading to final panel failure as shown in Figure 11. Although review of a video tape taken during the final pressure cycle is inconclusive, it is believed that final failure was precipitated by failure of one or both of the frames behind the growing crack. The crack was observed to commence growth at a differential pressure of 0.2 psi (0.001 MPa) below the maximum pressure achieved during the test. Prior to final failure, the crack extended about 3 inches (76 mm).

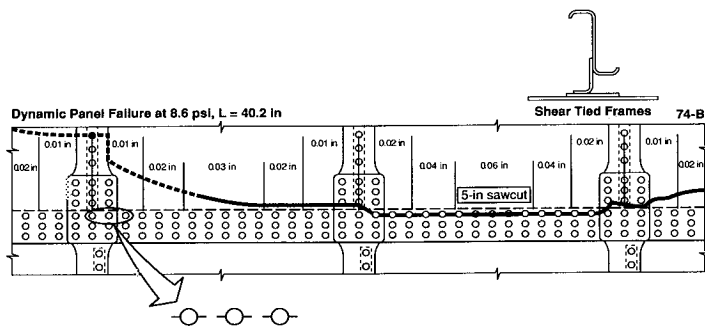


Figure 9. Multiple site damage test on panel 74-B lap joint.



Figure 10. Crack progression immediately prior to final failure of panel 74-B.

Review of Figure 11 shows the benefit of the fusing arrangement. The frames at the upper and lower ends of the cutout broke cleanly away from the test fixture. Similarly, the stringers separated cleanly along the

vertical edges of the cutout. It can also be observed that the frames in the central region of the test panel failed at a location consistent with the last fastener in the shear-tie.

Note that in neither panel 74-A nor 74-B did the small sawcuts ahead of the main crack significantly contribute to panel failure.

A number of additional tests of cracks in lap joints in narrow-body panels are summarized in the chart in Figure 12. The data expand on results previously presented in Reference 2. All pressure cycling was at a differential pressure of 7.8 psi (.054 MPa). The illustrations in the figure describe schematically the behavior of the cracks. Some of the tests, as noted on the figure, contained multiple site damage (MSD) in the fastener holes ahead of the lead crack. A controlled decompression occurred during the first test on panel 28A only. This panel did not include any MSD. In all other cases, the lead crack continued to grow in an essentially longitudinal direction throughout the test. However in several cases, similar to Test 74-B discussed above, the crack grew out of the lap joint into the basic skin before final panel failure. No clear trends emerge from these results. However, it does appear that MSD forces the lead crack to stay in the upper fastener row of the lap joint for a longer period of time. Comparison of Test 2 on panel 28A and the test on panel 27A shows that panel behavior is independent of the method of attaching the tear strap to the skin. However, it should be noted that the tear strap is spliced using rivets at the lap joint location in such a way that both the riveted and bonded designs are locally similar.

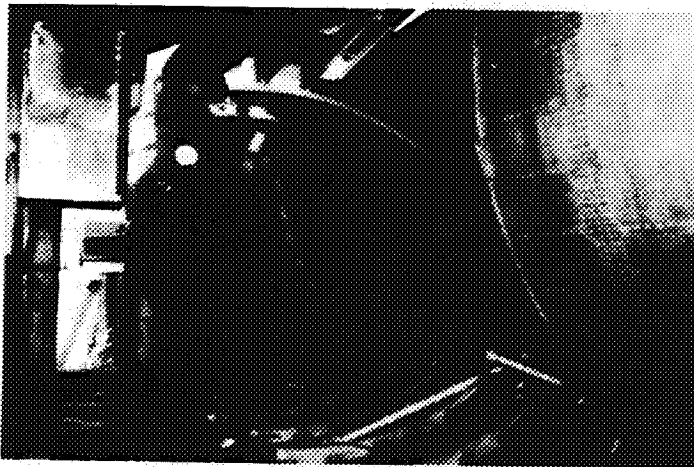


Figure 11. Final failure of panel 74-B.

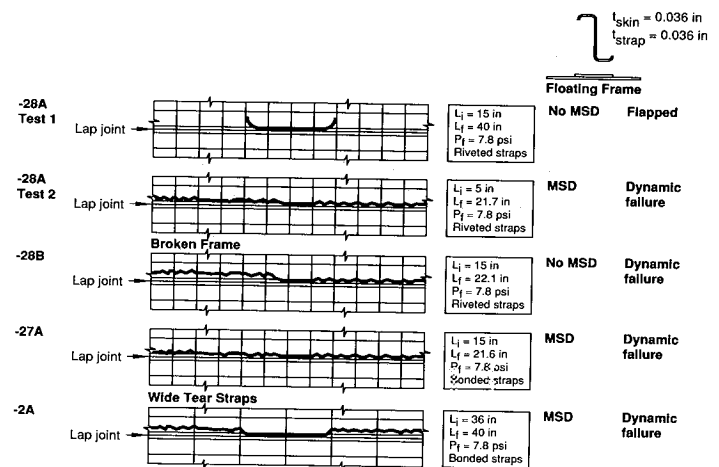


Figure 12. Summary of miscellaneous narrow-body lap joint crack growth tests.

Wide-Body Tests

A comparison of the effects of MSD on two wide-body panels is presented in Figure 13. The panels (127-B and 127-D) are 127 inch (3.23 m) in radius with frames and tear straps at a 20 inch (508 mm) spacing. The tear straps are bonded to the skin and have a stiffness ratio R_s of 0.12. The skin is 0.063 inch (1.6 mm) 2024-T3 clad sheet with the lap joint parallel to the longitudinal grain direction. The frames are shear-tied to the skin as illustrated in the figure. In each test, an initial sawcut of 5 inches (127 mm) was introduced into the upper row of fasteners in the lap joint and into the central tear strap. The central frame initially remained intact. In one case, MSD of the lengths shown in the illustration was introduced ahead of the lead crack. Each panel was subjected to fatigue cycling at a differential pressure of 8.6 psi (.059 MPa). When the cracks reached a length of 37 inches (940 mm), a differential pressure of 9.5 psi (.066 MPa) was applied. In each

case, this resulted in a small amount of crack extension. The central frame was cut and the pressure increased until panel failure. The panel with the MSD ahead of the lead crack failed at a differential pressure of 9.4 psi (.065 MPa), approximately 10% below the maximum differential pressure applied to the panel without MSD.

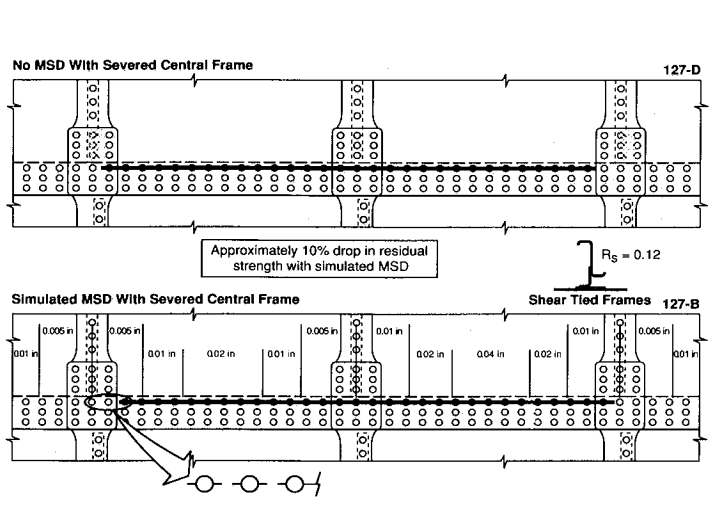


Figure 13. Effect of multiple site damage in lap joint on residual strength of wide-body panels.

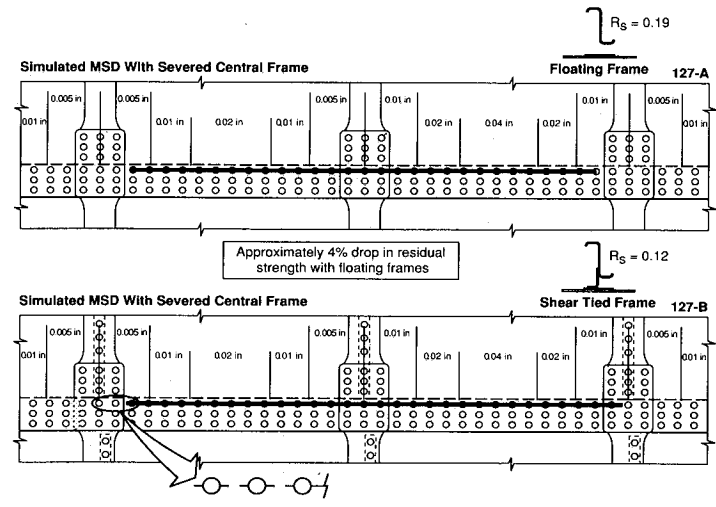


Figure 14. Effect of frame detail design on residual strength of wide-body panels with multiple site damage in lap joints.

The different capability of shear-tied against floating frame designs is illustrated in Figure 14. Test panel 127-B is as described in the previous paragraph. Test panel 127-A is similar with the exception that the frames are not shear-tied to the skin. The tear straps are bonded to the skin and have a stiffness ratio R_s equal to 0.19. The test procedure for panel 127-A was similar to 127-B with MSD introduced into the panel ahead of the lead crack as shown in the figure. This panel was subjected to fatigue cycles at a differential pressure of 8.6 psi (.059 MPa). When the crack reached a length of 37 inches (940 mm), a differential pressure of 9.5 psi (.066 MPa) was applied. Following this, the central frame was cut and the panel pressurized to failure. The condition of the panel prior to the final pressurization cycle and following the final cycle is illustrated in Figures 15 and 16.



Figure 15. Crack progression during multiple site damage test on wide-body panel 127-A lap joint.

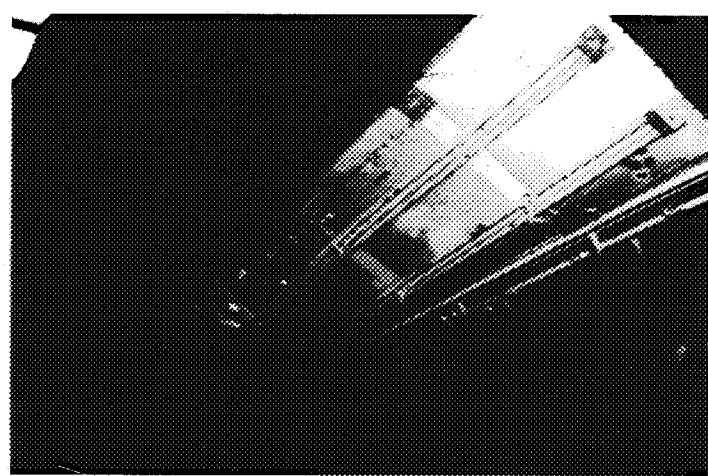
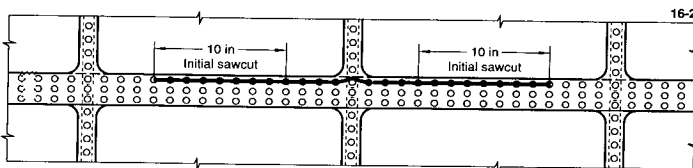


Figure 16. Final failure of multiple site damage test on panel 127-A lap joint.

The floating frame panel failed at 9.0 psi, approximately 4% less than the shear-tie panel. While this small difference could be attributed to test scatter, it is notable that this occurred despite the higher tear strap stiffness ratio. It is believed that the difference is associated with the ability of the shear-tied design to reduce the effects of out-of-plane displacements, or bulging, and to hold the crack closed.

Conceivably, MSD could occur in two or more adjacent bays. A single test on panel 16-2 was conducted to investigate the interaction of two large cracks in adjacent bays as shown in Figure 17. This panel was 127 inch (3.23 m) in radius. The skin was 0.075 inch (1.9 mm) C188-T3 clad aluminum with the lap joint parallel to the longitudinal grain direction. The panel was padded to a thickness of 0.1 inch (2.5 mm) at the lap joint. The frames were shear-tied to the skin which is locally padded to 0.1 inch (2.5 mm). Two 10 inch (254 mm) sawcuts were introduced into the upper row fasteners of the lap joint in the centers of two adjacent bays. The panel was loaded to a differential pressure of 8.6 psi (.059 MPa). The cracks were extended by sawcut one fastener at a time until each crack was about 15 inches (381 mm) in length and each crack tip was 1.25 inches (31.8 mm) from the centerline of the central shear-tie frame. At this time, 100 fatigue cycles at a differential pressure of 8.6 psi (.059 MPa) were applied to the panel. Subsequently, small sawcuts were introduced into the fastener holes to encourage re-initiation. After a further 11 fatigue cycles at the same differential pressure, the cracks linked up to form a single continuous crack of length 32.7 inches (830 mm). The test was discontinued following further fatigue cycling when the crack reached a length of 47.9 inches (1.22 m). The final condition of the crack is illustrated in Figure 18. While not conclusive, the test data indicate that cracks in adjacent bays do not automatically create an MSD concern.



- Sawcuts were extended one fastener at a time.
- 100 cycles applied once cracks were 1.25 in from the center shear tie rivets.
- A 0.006-in-wide blade was used to sharpen the tip approximately 0.05 in out of fastener holes.
- Cracks joined 11 cycles later.

Figure 17. Test details for large interacting cracks in lap joint of wide-body panel 16-2.

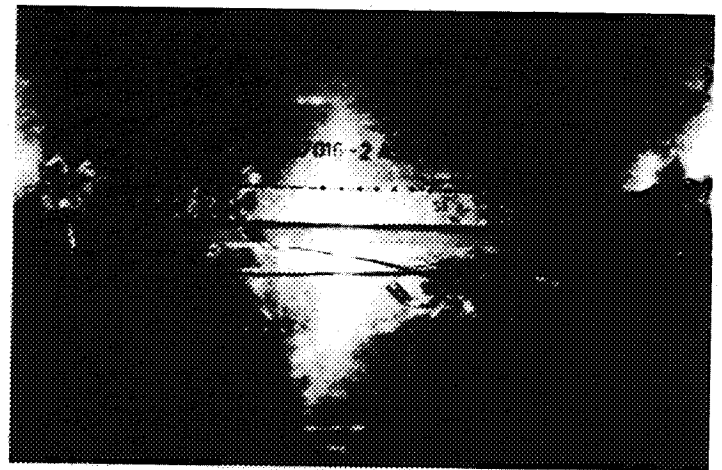


Figure 18. Final configuration of crack in lap joint of panel 16-2.

ANALYSIS PROCEDURE

The primary purpose of the analysis program is to predict the behavior of the test panels. This includes the test panel stresses (to be compared with strain gage data), the trajectory of crack growth from a sawcut, the crack growth life, and the residual strength. Residual strength can be the critical crack length under operating differential pressure or the maximum possible differential pressure for a given crack length. Successful comparisons will increase confidence in the analysis for predicting the behavior of typical fuselage structure containing cracks and for design studies.

Finite element models include the following test panel components: skin, tear straps, stringers and frames, stringer clips that attach the frames to the stringers, and, if present, shear ties that attach the frames to the skin. Eight-noded shell elements are used for the skin and tear straps, quadratic beam elements for the stringers and frames, shell elements for the shear ties, and rigid connections for the stringer clips. Fasteners are modelled with springs and rigid connections as discussed in Reference 1. Beam section coordinates are input into the model so that the nodes along the stringers are at the fastener locations and not at the neutral axis. In some cases, the tear straps are adhesively bonded to the skin. Early analysis attempts modeled the skin plus tear straps as one layer of thick shell elements. The resulting bending stresses did not correlate well with the test panels. Good results have been obtained by using two layers of shell elements. The adhesive layer is modeled with springs and rigid connections at all nodes, similar to the technique used to model riveted fasteners.

In most models, linear elastic material properties are used. In the residual strength models, material plasticity is introduced to selected elements. All analyses have been solved with ABAQUS using a geometric nonlinear solution sequence. A global analysis approach has been used so that fasteners and multiple site damage are not modelled explicitly.

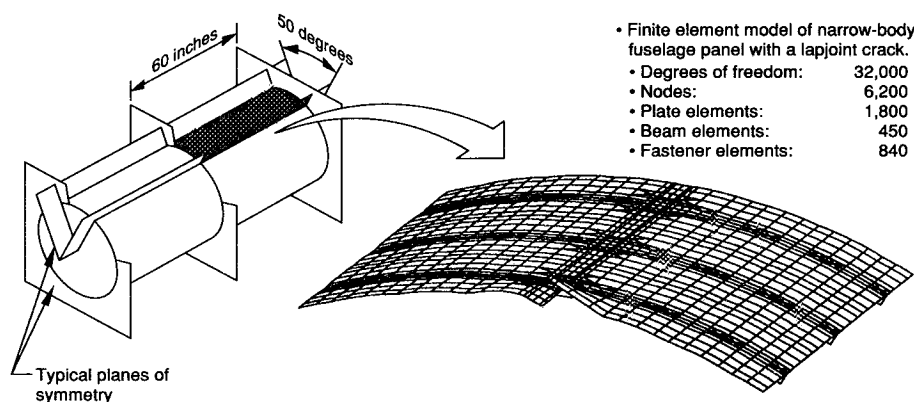


Figure 19. Finite element model of narrow-body test panel with lap joint.

A typical mesh for a narrow-body test panel containing a lap joint is shown in Figure 19. Only half of the test panel is modelled; a plane of symmetry is assumed at the crack centerline. Cylindrical symmetry is assumed at all boundaries. The circumferential boundary at the crack centerline is fixed in the longitudinal direction while the circumferential boundary away from the crack is allowed to displace uniformly in the longitudinal direction. The resultant of the pressure load in the longitudinal direction is applied at a node on this boundary.

A square-root singularity is assumed at all crack tips. Material plasticity at the crack tips is not considered since stress intensity factors are used as the basis for comparison with the experimental results. The square-root singularity is introduced into the ABAQUS models by use of collapsed eight-noded shell elements with quarter-point nodes surrounding the crack tips. Stress intensity factors are calculated using the displacements at nodes on the crack near the crack tip.

ANALYSIS RESULTS

A comparison between measured and predicted membrane hoop stresses for a narrow-body panel with floating frames is given in Figure 20. Bonded tear straps of stiffness ratio R_s equal to 0.15 coincide with the

frame locations. The data are for locations along an axial line midway between stringers and are presented in terms of the nominal hoop stress in an unstiffened cylinder of the same radius and skin thickness. The peak stress is observed to be about 85% of nominal and occurs midway between frames. The stress in the vicinity of the bonded tear straps falls to 60% of nominal. A good comparison of stresses can be observed at all locations.

A comparison between measured and predicted membrane hoop stresses in the vicinity of a lap joint in a narrow-body panel is given in Figure 21. The structure consists of floating frames at a 20 inch (508 mm) pitch and riveted tear straps at a 10 inch (254 mm) pitch. The tear strap stiffness ratio R_s is equal to 0.15. The data are for locations along an axial line adjacent to the lap joint. The data are presented in terms of the nominal hoop stress in an equivalent unstiffened cylinder of the same radius and lap joint skin gage thickness. The maximum stress of 80% of nominal occurs midway between the tear straps. A good comparison between test and analysis is obtained at this location. The stresses do not compare well at the tear straps. This may be caused by local bending at the skin and tear strap interface, or the influence of local stress concentrations around the fastener holes in the tear strap. The geometry of this panel model is similar to the test panels shown in Figure 12. Analysis results for this panel containing a 21.4 inch (540 mm) longitudinal crack show that the residual strength of the panel would be exceeded if the tear strap was broken.

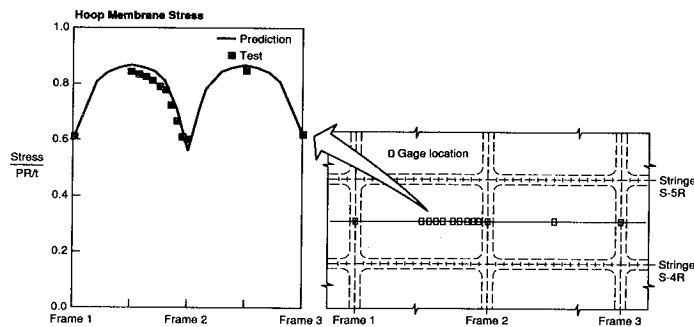


Figure 20. Test and analysis correlation for intact narrow-body panel 45-2A.

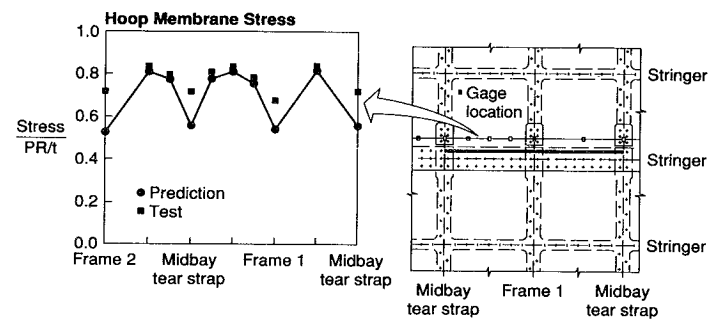


Figure 21. Test and analysis correlation for intact narrow-body panel 28-A adjacent to a lap joint.

A similar comparison of stresses is given in Figure 22 for the same panel containing a 20 inch (508 mm) crack in the upper row of fasteners in the lap joint and a broken central tear strap. As expected both measured and predicted hoop stresses behind the crack tips are close to zero. There are significant compressive membrane hoop stresses in the skin at the location of the broken tear strap. This is caused by local bending at the skin and tear strap interface. High tension stresses exist in the skin just ahead of the crack tip. Comparison with the data in Figure 21 shows the stresses are close to typical for the uncracked structure by the adjacent frame location (Frame 2 in the figure).

Panels 74-A and 74-B, discussed at length in the previous section, have also been the subjects of extensive analysis. A comparison of membrane stresses in the vicinity of the lap joint is given in Figure 23 for panel 74-B. The lap joint contains a 20 inch (508 mm) crack centered on the adjacent frame bay. The data are again presented in terms of the nominal hoop stress in an equivalent uncracked, unstiffened cylinder of the same radius and lap joint skin gage. The stresses are observed to be close to those for uncracked structure at the same locations.

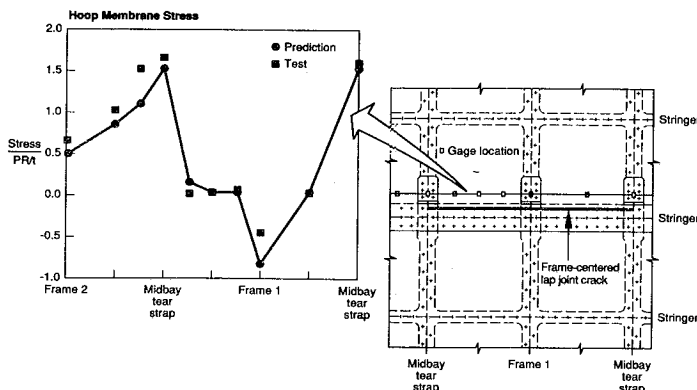


Figure 22. Test and analysis correlation for intact narrow-body panel 28-A containing a lap joint crack.

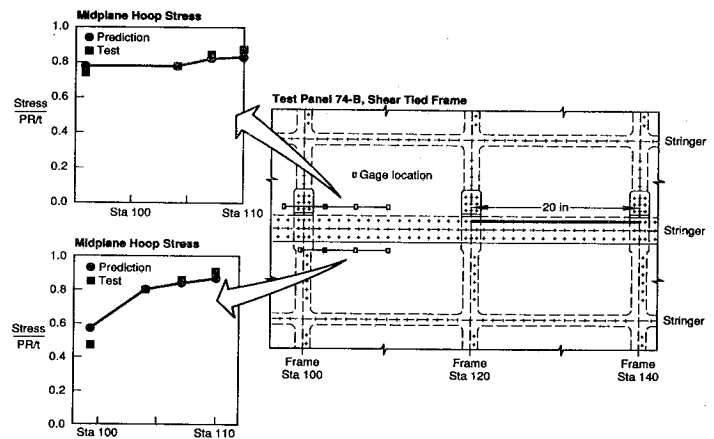


Figure 23. Test and analysis correlation for narrow-body panel 74-B containing a bay-centered lap joint crack.

Membrane stress intensity factors, non-dimensionalized with respect to the nominal membrane stress in an equivalent unstiffened cylinder, are presented in Figure 24 for panels 74-A and 74-B. Although the crack is along a lap joint, the fasteners and fastener holes are modeled only as point connections. Therefore, the stress intensity factors must be considered an approximation for lap joint configurations. It should be noted that the tear strap stiffening ratio R_s for the floating-frame panel is 0.19 and for the shear-tied panel, 0.12. Opening and sliding mode stress intensity factors are shown in the figure. In general, the opening mode stress intensity factor for the floating-frame panel is higher than for the shear-tied panel, even with the higher strap stiffness ratio. It is evident that the shear-tie helps to minimize the effect of out-of-plane displacements and to redistribute the loads around the crack. The effect of the broken tear strap is significant, causing a factor of three increase in opening mode stress intensity factor for cracks around 25 inches (635 mm) in length.

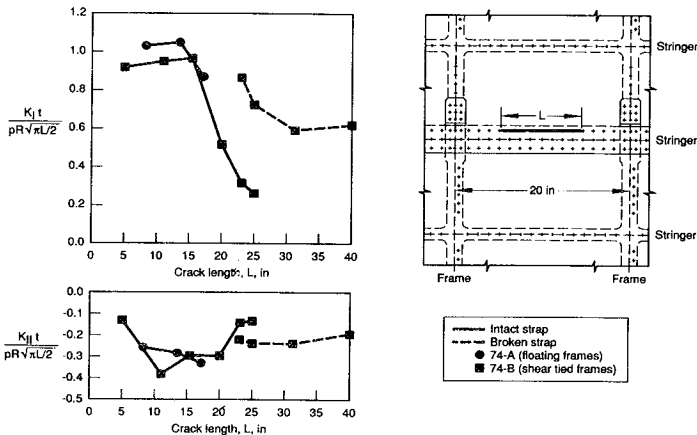


Figure 24. Non-dimensional stress intensity factors for narrow-body panels containing lap joint cracks.

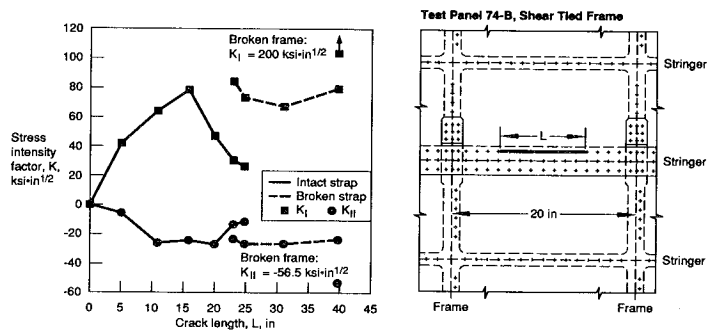


Figure 25. Stress intensity factors for narrow-body panel 74-B containing a lap joint crack.

The same data are presented as total opening and sliding mode stress intensity factors in Figure 25 for Panel 74-B. The opening mode stress intensity factor reaches a maximum of $78 \text{ ksi}\cdot\text{in}^{1/2}$ ($86 \text{ MPa}\cdot\text{m}^{1/2}$) when the skin crack is around 15 inches (380 mm) in length, before dropping as the tear strap is approached. The plane-stress fracture toughness for 0.04 inch (1.02 mm) clad 2024-T3 skin with cracks in the T-L orientation is in the range $120\text{-}130 \text{ ksi}\cdot\text{in}^{1/2}$ ($130\text{-}140 \text{ MPa}\cdot\text{m}^{1/2}$). As indicated in the discussion of the test results for this panel and as

illustrated in Figure 9, the crack remained sub-critical throughout this phase of the test. The tear straps failed in fatigue when the skin crack was 24.5 inches (620 mm) in length. At this point, the opening mode stress intensity factor in the skin was calculated to be $82 \text{ ksi}\cdot\text{in}^{1/2}$ ($90 \text{ MPa}\cdot\text{m}^{1/2}$), again well below the material toughness. The opening mode stress intensity factor is predicted to remain well below the material toughness with an intact frame. Following frame failure at a crack length of 40.2 inches (1.02 m), the opening mode stress intensity factor rises to $200 \text{ ksi}\cdot\text{in}^{1/2}$ ($220 \text{ MPa}\cdot\text{m}^{1/2}$), now well above the toughness of the material. The sliding mode stress intensity factor is presented for an assumed straight crack. This can be seen to remain fairly constant at around $25 \text{ ksi}\cdot\text{in}^{1/2}$ ($28 \text{ MPa}\cdot\text{m}^{1/2}$) for cracks longer than 10 inches (250 mm) in length, but rises significantly following frame failure.

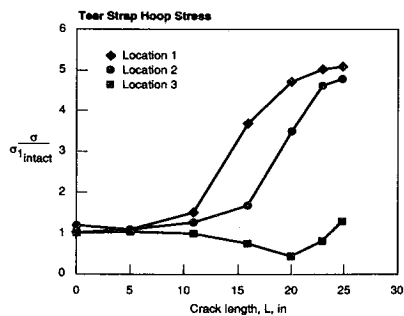
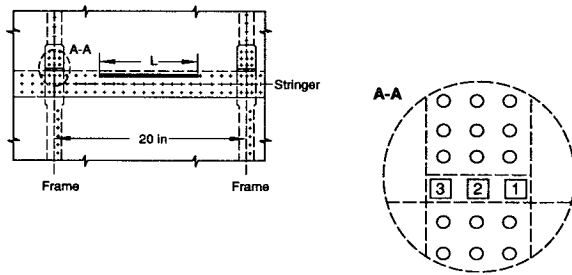


Figure 26. Stress concentration factors in tear strap for panel 74-B containing a lap joint crack.

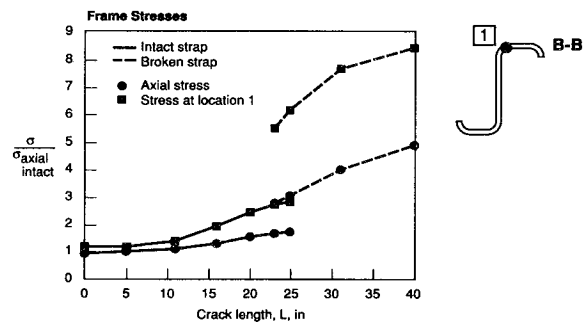
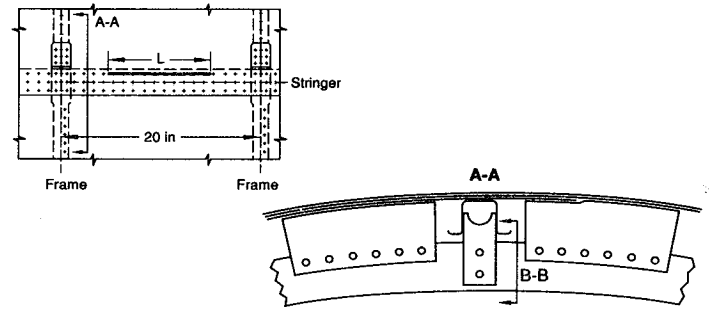


Figure 27. Stress concentration factors in frame for panel 74-B containing a lap joint crack.

The predicted tear strap stresses as a function of crack length, non-dimensionalized with respect to the stresses in the intact structure, are presented in Figure 26 for Panel 74-B. At short skin crack lengths, the stresses are uniform across the tear strap. As the crack approaches, the tear strap is subject to considerable bending in its plane. One side of the tear strap commences to yield when the skin crack is around 18 inches (460 mm) in length. In the test, the first fatigue crack was found in one of the straps when the skin crack was 20 inches (508 mm) in length. Insufficient data are available to reliably predict the fatigue life under such circumstances; however the tear straps failed in about 100 cycles during the test. Since the tear straps failed when the skin crack was 24.5 inches (620 mm) in length, no attempt was made to evaluate the tear strap stress concentration factors at longer skin crack lengths.

The predicted frame stresses as a function of crack length, non-dimensionalized with respect to the frame stresses in the intact structure are presented in Figure 27 for Panel 74-B. The stresses are provided at two locations. The first represents the average axial stress in the frame and the second represents the peak fiber stress in the outer chord of the frame just beyond the last shear-tie attachment fastener. At short skin crack lengths, the increase in stress in the frame is small. As the crack length increases, the stresses in the frame at both locations steadily increase but remain well below yield for the 7075-T6 frame material. Following tear

strap failure, the axial stress in the frame increases by about 50% but the peak fiber stress increases by 100%, indicating a significant increase in frame bending. The stresses remain below yield in the material (a yield stress of 68 ksi (470 MPa) was assumed in the analysis) until the skin crack exceeds about 35 inches (890 mm) in length. When the skin crack length is 40 inches (1.02 m), close to final panel failure, the nominal peak fiber stress in the frame exceeds 70 ksi (480 MPa). Final failure, illustrated in Figure 10, was through the last shear-tie attachment fastener. The peak fiber stress coupled with the stress concentrating effect of the fastener hole may have been sufficient to precipitate a static failure, or in a fashion similar to the tear strap, a very low-cycle fatigue failure. No observations of any fatigue cracks in the frame were recorded during the test.

A comparison between predicted and measured frame stresses in Panel 74-B is given in Figure 28. Axial stresses near the center of the frame channel, midway between two stringers are provided for two locations. The first is in the bay containing the crack and the second is in the adjacent bay, as illustrated in the figure. Stresses compare favorably while the tear strap is intact. Following tear strap failure, analysis stresses tend to be high in the bay containing the crack and low in the adjacent bay. Review of the analysis suggests that since the stringer clip attaching the stringer to the frame is modeled as a rigid connection, inaccurate predictions of load transfer into the frame result.

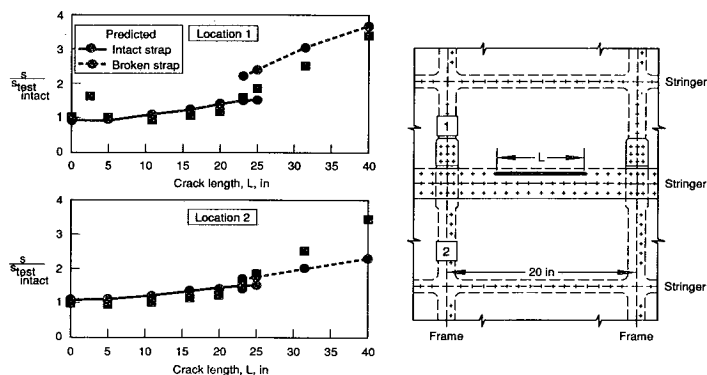


Figure 28. Comparison between test and predicted axial stresses in frame for panel 74-B as a function of skin crack length.

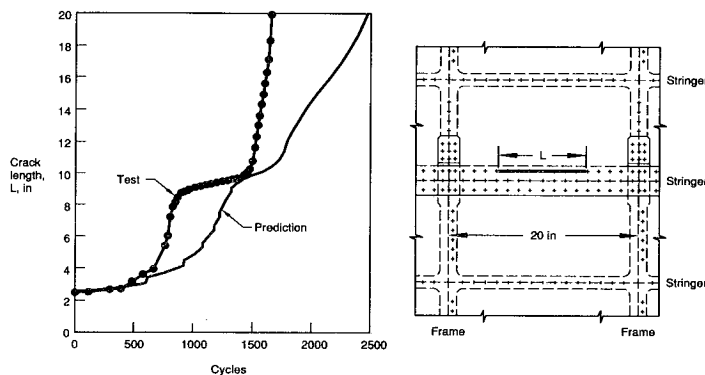


Figure 29. Comparison between test and predicted crack growth for panel 74-B containing a lap joint crack.

A comparison of skin fatigue crack growth lives for Panel 74-B is shown in Figure 29. In general, the prediction follows the test but tends to overestimate the life by about 50%. The analysis assumed fasteners behaved elastically at all times. In view of the high stresses calculated for the tear straps and frames, it is certain that several fasteners would have exceeded their yield strength. As a result, the stress intensity factor in the skin is likely to be greater than shown in Figure 25, especially for cracks beyond 20 inches (508 mm) in length. This may account for the observed differences between predicted and measured crack growth rates at the longest crack lengths.

Fully automated remeshing schemes for curving cracks are not yet available within Boeing although such a capability is under development such as the effort described in Reference 3. As a result, only a few attempts to predict crack trajectories have been made. One such attempt was made on Panel 45-2A. This narrow-body panel consisted of .036 inch (0.9 mm) 2024-T3 skin with 3 inch (76 mm) wide bonded tear straps, R_s equal to 0.15, at a 20 inch (508 mm) pitch. The panel had floating frames coincident with the tear straps. The initial damage in the panel consisted of a 5 inch (127 mm) sawcut across and including a broken tear strap. Predicted

crack trajectories are based on the maximum strain energy release rate. The predicted and measured crack trajectories are shown in Figure 30 to be in good agreement at all crack lengths. Final failure in this panel was by means of a controlled decompression. It can be observed that this failure mode can occur without the beneficial influence of nearby tear straps.

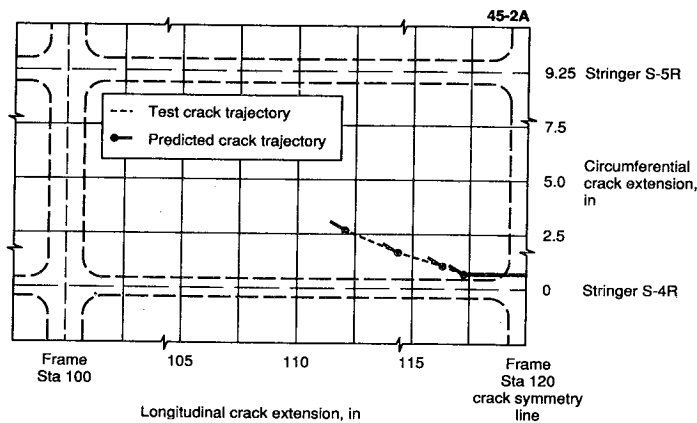


Figure 30. Comparison between test and predicted crack trajectory for narrow-body panel 45-2A containing a longitudinal crack.

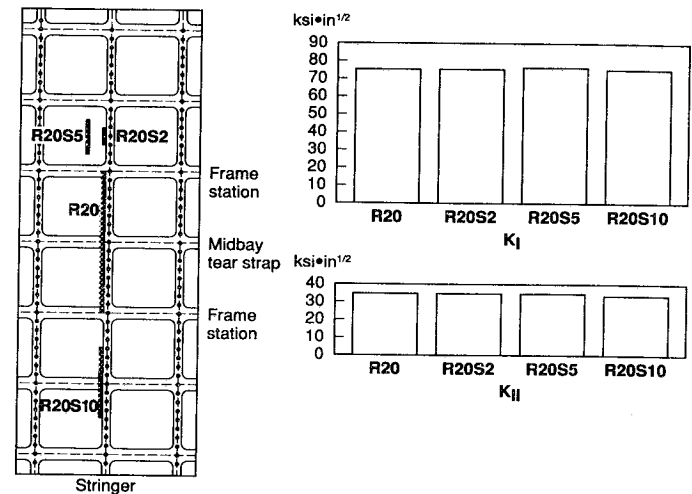


Figure 31. Effect on stress intensity factors of large interacting longitudinal cracks in a narrow-body panel.

An analysis of the interaction of large cracks in adjacent bays is given in Figure 31. The narrow-body panel consists of .036 inch (0.9 mm) thick 2024-T3 clad skin, tear straps with an R_s of 0.15 at 10 inch (254 mm) pitch, and floating frames at 20 inch (508 mm) pitch. An axial crack of length 20 inches (508 mm) centered on a broken tear strap is introduced into the structure adjacent to a stringer. An analysis is conducted for each of the different length secondary cracks located as shown in the figure. Because of the symmetry of the analysis model, each secondary crack occurs twice. Thus analysis R20S10 describes a 10 inch (254 mm) crack 5 inches (127 mm) ahead of each tip of the 20 inch (508 mm) crack. The opening and sliding mode stress intensity factors for the lead crack are shown in bar chart form for each of the crack configurations. In every case, the influence of the secondary cracks on the primary crack is negligibly small.

CONCLUSIONS AND RECOMMENDATIONS

Recent test and analysis results from an investigation into the behavior of cracks in typical fuselage structure have been discussed. In general, this has led to an increased understanding of our current capabilities. Some specific conclusions and recommendations follow.

Use of air as a pressurizing medium is necessary if the true dynamic conditions of a crack growing in representative fuselage structure are to be adequately assessed. However the risks associated with this type of testing need to be properly understood and adequate safeguards taken. Filling the cavity with polystyrene blocks and other similar material helps reduce cycling time but does not significantly reduce the energy stored in the test article. Greater air compressor capacity would help reduce cycling time. Air loss during fatigue cycling with long cracks needs to be addressed but rubber bladders have proven to be effective without significantly altering the progress of the crack through the structure. A fusing arrangement around the periphery of the test panel allows residual strength testing to destruction while minimizing damage to the test fixture.

Video recording of tests has proven to be extremely valuable, both in real time to monitor the progress of the crack allowing quick decisions to be made as the load is increased during residual strength testing, and as a permanent record for later evaluation. Strategically located strain gages also allow real-time monitoring of critical structural elements during residual strength testing.

The testing conducted to date indicates that longitudinal cracks in wide-body fuselage sections tend to grow in fatigue in a generally longitudinal direction, and do not result in a controlled decompression. On the other hand, similar cracks in narrow-body structures curve to grow circumferentially in about 50% of the cases. Exceptions are cracks midway between stringers. For the MSD pattern explored in wide-body panels with shear-tied frames, the residual strength was reduced by 10%, a smaller reduction than indicated by flat, unstiffened panel testing (see, for example, Reference 2). In narrow-body panels, the tendency of the lead crack to curve often negates the effect of MSD on final failure. Large skin cracks in adjacent frame bays need to be in close proximity before significant interaction is evident.

Structures in which the frames are tied to the skin by means of shear-ties appear to be more damage tolerant than structures with floating frames. However, additional evaluation of the relative structural efficiency needs to be conducted.

Insufficient data were available to accurately predict the fatigue life of tear straps and frames under very-low cycle fatigue conditions. Service experience shows that airline maintenance practices are more than adequate for finding long, externally visible cracks should they occur. The additional opportunities afforded by crack arrest features, such as tear straps and shear-ties, having good fatigue performance will increase opportunities for crack detection.

Future testing will include more head-to-head comparisons of cracked lap joints with or without MSD to fully characterize the loss of residual strength that might be expected. This will aid development of methods for predicting the point at which the performance of the cracked structure falls below acceptable levels. Development of a method for evaluating lap joints can then be applied to other structure susceptible to MSD for which suitable test facilities are unavailable.

Although not a primary focus of the testing discussed in this paper, the benefits to residual strength of well-bonded tear straps need to be further explored. As expected, bonded tear straps more effectively transfer load around a crack than riveted tear straps in most comparative tests. In particular, the resistance of the adhesive interface to disbonding as the crack in the skin tunnels under the tear strap needs to be understood.

A failure criterion for curving cracks in thin shells has yet to be established. While it has been shown that failure by controlled decompression is common in some typical fuselage structure, no method for sizing of structural elements such as tear straps to guarantee this type of failure is available.

Designers often increase the skin thickness of fuselage lap joints to increase the fatigue life. The effect of this local design feature on the damage tolerance of lap joints has not been the subject of systematic study, especially if the potential for MSD exists.

While the analysis approach described in this paper is more than adequate for typical structure, it is not a practical tool for the detail examination of local effects, such as loaded fastener holes and secondary bending,

that would occur in a lap joint. As a result, no attempt has been made to investigate analytically the interaction of small cracks ahead of a large crack in a lap joint.

In general, good correlation has been demonstrated between test and analysis for both intact and cracked structure. Trends observed in tests have also been confirmed by analysis. These include the observations that longitudinal cracks midway between stringers grow faster than cracks near stringers; that large cracks in adjacent frame bays do not interact significantly; and that panels with shear-tied frames tend to resist damage growth better than panels with floating frames. Crack growth rate comparisons presented in this paper and in Reference 1 are generally good at crack lengths less than 20 inches, but tend to become less satisfactory at longer lengths. The causes have not been completely identified but may include inaccurate crack growth rate data at very high stress intensity factors, or a need for additional elastic-plastic modeling of key structural elements such as fasteners, tear straps, shear-ties and stringer clips. The effects of these elements on fatigue crack growth and residual strength have been investigated for some test panels. In general, they can exceed yield as any damage approaches critical dimensions. An improved fastener load transfer model would increase confidence in the analysis of the behavior of very long cracks. The need to include skin plasticity has yet to be examined.

Future analyses will continue to focus on available test panel configurations, but will be expanded to include more parametric studies. Global-local modeling techniques will be employed to gain a better understanding of the effects of multiple site damage. Modified energy equations that include bending stress intensity factors will also be investigated to determine how they affect fatigue crack growth and residual strength.

REFERENCES

1. Miller M., Kaelber K. N., Worden R. E., "Finite Element Analysis of Pressure Vessel Panels," International Workshop on Structural Integrity of Aging Airplanes, 31 March -2 April 1992, Atlanta, Ga., USA.
2. Maclin J. R., "Performance of Fuselage Pressure Structure," Third International Conference on Aging Aircraft and Structural Airworthiness, November 19 - 21, 1991, Washington, D.C., USA.
3. Potyondy D., "A Software Framework for Simulating Curvilinear Crack Growth in Pressurized Fuselages," Doctoral Dissertation, Cornell University, 1993.

ACKNOWLEDGMENTS

The authors would like to acknowledge the graphics and publications support from Mr. W. J. Brewer and from Boeing Support Services.